Physics of the Earth and Planetary Interiors 229 (2014) 122–133

Contents lists available at ScienceDirect

Physics of the Earth and Planetary Interiors

journal homepage: www.elsevier.com/locate/pepi

Magnetic reversal frequency scaling in dynamos with thermochemical convection

Peter Olson [a,*], Hagay Amit [b]

[a] Department of Earth and Planetary Sciences, Johns Hopkins University, Baltimore, MD 21218, USA
[b] CNRS UMR 6112, Université de Nantes, Laboratoire de Planétologie et de Géodynamique, 2 rue de la Houssinière, Nantes F-44000, France

ARTICLE INFO

Article history:
Received 19 August 2013
Received in revised form 10 January 2014
Accepted 16 January 2014
Available online 1 February 2014
Edited by C. Jones

Keywords:
Geodynamo
Polarity reversals
Core convection
Geomagnetic dipole
Core–mantle boundary

ABSTRACT

Scaling relationships are derived for the frequency of magnetic polarity reversals in numerical dynamos powered by thermochemical convection. We show that the average number of reversals per unit of time scales with the local Rossby number Ro_ℓ of the convection. With uniform core–mantle boundary (CMB) heat flux, polarity reversals are absent below a critical value $Ro_{\ell crit} \simeq 0.05$, beyond which reversal frequency increases approximately linearly with Ro_ℓ. The relative standard deviation of the dipole intensity fluctuations increases with reversal frequency and Ro_ℓ. With heterogeneous CMB heat flux that models the large-scale seismic heterogeneity in Earth's lower mantle, reversal frequency also exhibits linear dependence on Ro_ℓ, and increases approximately as the square root of the amplitude of the CMB heterogeneity. Applied to the history of the geodynamo, these results imply lower CMB heat flux with $Ro_\ell \leqslant Ro_{\ell crit}$ during magnetic superchrons and higher, more heterogeneous CMB heat flux with $Ro_\ell > Ro_{\ell crit}$ when geomagnetic reversals were frequent. They also suggest that polarity reversals may have been commonplace in the early history of other terrestrial planets. We find that zonal heterogeneity in CMB heat flux produces special effects. Close to $Ro_{\ell crit}$ enhanced equatorial cooling at the CMB increases reversal frequency by concentrating magnetic flux at low latitudes, whereas far beyond $Ro_{\ell crit}$ enhanced polar cooling at the CMB increases reversal frequency by amplifying outer core convection.

1. Introduction

Many of the larger objects in the solar system have experienced dynamo action at some time in their history, but among the planets, only the Earth has a record of magnetic polarity reversals. Paleomagnetic data shows that polarity reversals have occurred throughout Earth's history since the Archean (Layer et al., 1996; Strik et al., 2003), with the length of time between reversals having varied by nearly three orders of magnitude, from 40 Myr long superchrons to short subchrons lasting under 40 kyr (Cande and Kent, 1995; Merrill et al., 1998). It remains an open question as to whether the histories of other planetary dynamos include polarity transitions.

The general criteria that determine under what conditions and how often a self-sustaining planetary dynamo undergoes spontaneous polarity reversals remain obscure, but the reversal behavior of numerical dynamos (Kutzner and Christensen, 2000; Kutzner and Christensen, 2002; Christensen and Aubert, 2006; Olson and Christensen, 2006; Aubert et al., 2009; Wicht et al., 2009), laboratory dynamos (Berhanu et al., 2007) and idealized theoretical models (Pétrélis et al., 2009; Gissinger et al., 2010) point to some of the conditions under which polarity transitions are favored. Numerical dynamo studies in particular have identified several factors that control the likelihood of reversals. On average, reversals are more likely as the dynamo forcing is increased (Heimpel and Evans, 2013), and conversely, they become less likely as the planetary rotation is increased (Kutzner and Christensen, 2002). The timing of the individual reversals appears to be largely stochastic (Olson et al., 2009; Wicht et al., 2009). Using low resolution dynamos that produce large sets of reversals, Driscoll and Olson (2009a) delineated the transition from stable to reversing dynamos in terms of the relative strengths of convection and rotation, and confirmed that increasing the vigor of convection or decreasing the rate of rotation tends to destabilize the polarity. Driscoll and Olson (2009a) also found that the frequency of reversals generally increases with the vigor of convection in dynamos with fixed rotation, and reversal frequency generally decreases when the rotation is increased but the convection is fixed. In addition, for dynamos with uniform boundary conditions, it has been found that the mean boundary heat flux is inversely proportional to dipole strength, so reversal frequency may be anti-correlated

* Corresponding author. Tel.: +1 410 516 7707.
E-mail address: olson@jhu.edu (P. Olson).

http://dx.doi.org/10.1016/j.pepi.2014.01.009
0031-9201/

to dipole strength (Driscoll and Olson, 2009b; Driscoll and Olson, 2011).

Based on numerical dynamos with heterogeneous core–mantle boundary (CMB) heat flux, it was proposed that the relationship between the background dynamo convection mode and the boundary pattern may influence dipole stability (Glatzmaier et al., 1999), and in particular, the latitudinal distribution of CMB heat flux can affect reversal frequency. Enhanced CMB heat flux inside the tangent cylinder promotes dipole stability (Glatzmaier and Roberts, 1997; Glatzmaier et al., 1999), enhanced equatorial heat flux increases reversal frequency (Glatzmaier et al., 1999; Kutzner and Christensen, 2004; Olson et al., 2010), whereas reduced equatorial heat flux decreases reversal frequency and may even prevent reversals (Glatzmaier et al., 1999; Kutzner and Christensen, 2004), although this latter result is not always replicated (Olson et al., 2010). Kutzner and Christensen (2004) found with a spherical harmonic degree Y_2^2 CMB heat flux pattern that reversal frequency varies linearly with convection vigor and nearly linearly with the amplitude of the boundary anomaly, but for tomographic conditions they found no variation of reversal frequency with convection strength or boundary heterogeneity amplitude. In contrast, Olson et al. (2010) and Heimpel and Evans (2013) found that increasing the boundary heterogeneity amplitude nearly always increases reversal frequency. Another important factor is the level of equatorial symmetry of the CMB heat flux, specifically, the possibility that high equatorial symmetry promotes dipole stability (Pétrélis et al., 2009; Pétrélis et al., 2011). In particular, laboratory reversing dynamos (Berhanu et al., 2007) point to the importance of symmetry breaking of the fluid motion in precipitating reversal onset.

Although moderate variations in reversal frequency are attributable to the stochastic nature of dynamo action (Jonkers, 2003; Ryan and Sarson, 2007; Wicht et al., 2009), the existence of superchrons in the paleomagnetic record and the fact that they are spaced about 200 Myr apart, similar to the overturn time of mantle convection, suggests that changing mantle conditions play some role (Glatzmaier et al., 1999; Kutzner and Christensen, 2004). Driscoll and Olson (2009b) proposed that the initiation and termination of a superchron requires an anomalous perturbation of the convective and rotational mean state of the core. Driscoll and Olson (2011) found that the CMB heat flux magnitude is positively correlated with reversal frequency, and argued on this basis that the superchron cycle is caused by slow variations in the magnitude of the CMB heat flux magnitude, as would result from time dependent mantle convection.

In this paper we measure reversal frequency in a set of low-resolution numerical dynamos in which the distribution of convective forcing is similar to what is inferred for the present-day geodynamo. In these numerical dynamos, the primary driving force is the flux of co-density at the inner core boundary (ICB), representing buoyancy produced by solidification of the inner core. In contrast, the heat flux at the CMB is comparable to the heat conducted along the core adiabat, so the contribution from thermal buoyancy to the convection is smaller than from compositional buoyancy. For purposes of generality, we consider dynamos with both uniform CMB heat flux, the basic model for terrestrial planets, plus dynamos with boundary heat flux heterogeneity. In one set of cases representing the present-day Earth, the CMB heterogeneity is proportional to the long wavelength seismic heterogeneity in the lower mantle, and in another set of cases representing hypothetical past conditions, the heterogeneity is proportional to a single spherical harmonic degree. We then derive scaling laws that link the reversal frequency in these types of dynamos to the local Rossby number of the convection and to the fluctuations of the dipole moment. Previous numerical dynamos studies have established that the onset of reversals have some connection with these parameters (Christensen and Aubert, 2006; Olson and Christensen, 2006; Sreenivasan and Jones, 2006; Aubert et al., 2009; Driscoll and Olson, 2009b; Wicht et al., 2009; Olson et al., 2010; Biggin et al., 2012; Gastine et al., 2012; Duarte et al., 2013) but did not provide a quantitative relationship between reversal frequency and these parameters.

2. Methods

We focus on numerical dynamos with dominantly compositional driving, and make use of the co-density formulation (Braginsky and Roberts, 1995) in which $C = \rho(\alpha T + \beta\chi)$ where ρ is mean density, T is temperature, χ is the light element concentration (mixing ratio) in the outer core, and α and β are their respective expansivities. Control parameters for these dynamos include the Ekman number E, the Prandtl number Pr and the magnetic Prandtl number Pm defined respectively by

$$E = \frac{\nu}{\Omega D^2} \tag{1}$$

$$Pr = \frac{\nu}{\kappa} \tag{2}$$

$$Pm = \frac{\nu}{\eta} \tag{3}$$

where ν is kinematic viscosity, Ω is the angular velocity of rotation, $D = r_o - r_i$ is the outer core shell thickness, κ is the diffusivity of the co-density and η is magnetic diffusivity. Buoyancy is parameterized in terms of the Rayleigh number Ra, which can be defined for thermochemical dynamos as

$$Ra = \frac{\beta g D^5 \dot{\chi}}{\kappa \nu^2} \tag{4}$$

where g is gravity at the CMB and $\dot{\chi}$ is the time rate of change of the light element concentration (mixing ratio) in the outer core due to inner core growth. Here we have used D and D^2/ν to scale length and time, respectively, and $\rho\beta D^2\dot{\chi}/\nu$ to scale co-density.

Boundary conditions lead to additional control parameters. At the ICB we set $C = C_i$. At the CMB we specify the heat flux as the sum of a global mean part $\bar{q}$ and a laterally varying part q':

$$q = \bar{q} + q'(\phi, \theta) \tag{5}$$

where ϕ and θ are longitude and co-latitude, respectively, and $\bar{q}$ is measured relative to the heat flux down the core adiabat, such that $\bar{q} > 0$ corresponds to superadiabatic heat flux. The function q' in (5) specifies the amplitude and the planform of the CMB heat flux heterogeneity.

In terms of the dimensionless radial coordinate r^* and the scaled global mean and laterally varying co-density $\overline{C}^* + C'^*(\phi, \theta)$, we write the flux conditions on the CMB as

$$\frac{\partial \overline{C}^*}{\partial r^*} = -\bar{q}^* \tag{6}$$

and

$$\frac{\partial C'^*}{\partial r^*} = -q'^* \tag{7}$$

where $\bar{q}^* = \alpha\nu\bar{q}/\beta k D\dot{\chi}$ is the dimensionless global mean CMB heat flux, $q'^* = \alpha\nu q'/\beta k D\dot{\chi}$ is its dimensionless lateral heterogeneity, and k is the thermal conductivity.

The dimensionless amplitude of the CMB heat flux heterogeneity is often expressed as one-half of the peak-to-peak boundary heat flux variation normalized by the mean (Olson and Christensen, 2002):

$$\delta q^* = \frac{q'_{max} - q'_{min}}{2\bar{q}} \tag{8}$$

However, $\bar{q} = 0$ for some thermochemical dynamos, so an alternative normalization is needed for these cases. Here we use the following dimensionless parameter to measure the amplitude of the boundary heterogeneity:

$$\delta q_c^* = \frac{\alpha \nu (q'_{max} - q'_{min})}{2\beta k D \dot{\chi}} \tag{9}$$

The final control parameter is ϵ, the sink (or source) term that appears in the co-density transport equation (Christensen and Wicht, 2007), which models the rate of mixing of light elements in the outer core, secular cooling of the outer core, curvature of the core adiabat, and radioactive heat sources, with $\epsilon = -1$ representing purely compositionally-driven convection.

In this study we further restrict consideration to dynamos with $Pr = 1$, relatively large E and Pm, negative ϵ appropriate for dominantly compositional convection, modest Ra, plus a range of $\bar{q}^*$ and q'^*. We set the aspect ratio to be $r_i/r_o = 0.35$. Both inner and outer boundaries are rigid and insulating. Previous experience with these dynamos have confirmed their "Earth-like" status in terms of magnetic field morphology (Christensen et al., 2010), their sensitivity to rotation, buoyancy, and CMB heterogeneity (Driscoll and Olson, 2009b, 2011; Olson et al., 2010) and their conformity to Poisson reversal statistics (Lhuillier et al., 2013). The rationale for compositionally-dominated convection in the outer core is strengthened by recent seismic studies (Helffrich and Kaneshima, 2010) and mineral physics calculations (Pozzo et al., 2012) that indicate the electrical and thermal conductivities in Earth's outer core are much larger than previously considered. Such large conductivities have significant implications for the thermal history of the core and its present-day buoyancy distribution, and imply that convection in the outer core is probably dominated by light element release at the ICB, with thermal buoyancy likely playing a secondary role and possible stratification at the top of the outer core (Gubbins and Davies, 2013).

For purposes of comparison with the paleomagnetic record and previous dynamo reversal studies, we express the average reversal rate in terms of the dipole free decay time

$$\tau_d = \frac{r_o^2}{\pi^2 \eta}, \tag{10}$$

so that if N denotes the number of reversals in a given time interval $\delta t = \tau_d \delta t^*$, the dimensionless reversal frequency is defined as

$$N^* = \frac{N\tau_d}{\delta t} = \frac{N}{\delta t^*} \tag{11}$$

Since it has already been shown that the times of individual reversals in these types of numerical dynamos conform to Poisson statistics (Lhuillier et al., 2013), an appropriate definition for the standard deviation of N^* is just (e.g. Wilks, 2006)

$$\delta N^* = \frac{\sqrt{N}}{\delta t^*} \tag{12}$$

Reversal frequency is related in a general way to the level of time variability in numerical dynamos, particularly the dipole field variability. Accordingly, we wish to relate N^* to an appropriate dimensionless measure of the dipole intensity fluctuations, for example, the ratio of the fluctuations to the mean intensity. To nondimensionalize the magnetic field intensity we use $\sqrt{\rho\mu\Omega\eta}$ (Elsasser number scaling), where μ is magnetic permeability. If B_d^* denotes the dimensionless time average of the rms dipole intensity on the CMB and δB_d^* denotes its standard deviation, the relative standard deviation of the dipole intensity is given by

$$\sigma^* = \frac{\delta B_d^*}{B_d^*}. \tag{13}$$

There are several parameters that are commonly used to describe the vigor of the dynamo-producing flow in the outer core, including the hydrodynamic Reynolds number, the magnetic Reynolds number, and several definitions of the Rossby number (Christensen and Aubert, 2006). For dynamo onset, it is well established that the key parameter is the global magnetic Reynolds number (Elsasser, 1956; Moffatt, 1978; Davidson, 2001; Roberts, 2007)

$$Rm = \frac{uD}{\eta} \tag{14}$$

defined in terms of the rms fluid velocity in the outer core u. However, this parameter is not a good choice for scaling reversals, because it does not properly factor in the effects of planetary rotation and inertia (Christensen and Aubert, 2006; Olson and Christensen, 2006; Aubert et al., 2009; Wicht et al., 2009). In convective dynamos, the axial dipole is maintained by columnar convection, a consequence of the dominance of the Coriolis effect (e.g. Christensen et al., 1998; Olson et al., 1999), and column breaking by inertial effects is commonly cited as a cause for reversals. According to this reasoning, the Rossby number defined by

$$Ro = \frac{u}{\Omega D} \tag{15}$$

would be appropriate for scaling reversals. However, this parameter is minute in the outer core, and furthermore, it fails to rationalize reversal behavior in numerical dynamos, evidently because the global length scale D in (15) does not reflect the actual length scale of the convection.

Accordingly, the global length scale D appearing in (15) should be replaced with a length scale that better reflects the characteristic size of the convective eddies in the outer core. Screening effects of crustal magnetization prevents inferring the characteristic eddy size of outer core convection from inversions of the geomagnetic secular variation (Holme, 2007), so the usual procedure is to infer it from the systematics of numerical dynamos (Christensen and Aubert, 2006; Olson and Christensen, 2006). Let ℓ_u be a characteristic spherical harmonic degree of the fluid velocity of the dynamo defined by

$$\ell_u = \sum_{\ell=0}^{\ell_{max}} \ell \frac{\langle \mathbf{u}_\ell \cdot \mathbf{u}_\ell \rangle}{\langle \mathbf{u} \cdot \mathbf{u} \rangle} \tag{16}$$

where $\mathbf{u}$ is the fluid velocity vector, $\mathbf{u}_\ell$ is the fluid velocity vector at harmonic degree ℓ, and the angle brackets denote volume average. The local Rossby number is then defined using (15) and (16),

$$Ro_\ell = \frac{u\ell_u}{\pi\Omega D} = \frac{\ell_u}{\pi} Ro. \tag{17}$$

The normalization factor π in the denominator of (17) was introduced by Christensen and Aubert (2006) and will be retained in our study.

3. Reversal scaling results

In this section we quantify the sensitivity of reversal frequency N^* to the local Rossby number Ro_ℓ by independently varying the control parameters in several types of thermochemical dynamos in which the reversal frequency is determined. Tables 1–3 give statistics from a large set of thermochemical dynamos described in the previous section. Run durations δt^* correspond to the number of dipole decay times τ_d, the dimensionless rms dipole intensity on the outer core boundary B_d^* and its standard deviation δB_d^* are in Elsasser number units, and N denotes the total number of reversals observed. We distinguish reversals from excursions based on their duration as in Olson et al. (2010). The last two columns in

Table 1
Numerical Dynamo Reversals Statistics. **U1**: Uniform, chemical, $E = 6\cdot10^{-3}$, $Pm = 20$, variable $Ra, \bar{q}^* = -0.1$, $\epsilon = -0.282$; **U2**: Uniform, chemical, $E = 5.75\cdot10^{-3}$, $Pm = 20$, variable $Ra, \bar{q}^*=0$, $\epsilon = -1.0$; **U3**: Uniform, chemical, variable $E, Pm = 20, Ra = 10,000$, $\bar{q}^* = 0.1, \epsilon = -1$; **U4** from Olson et al. (2012): Uniform, chemical, E =3e-4, $Pm = 3$, variable $Ra, \bar{q}^* = 0.1, \epsilon = -1$; **UT:** Uniform, base-heated, $E = 1\cdot10^{-3}$, $Pm = 5$, variable Ra; **T1**: Tomographic, thermochemical, $E = 5.75\cdot10^{-3}$, $Pm = 20$, variable $Ra, \bar{q}^* = -0.1$, $\delta q_c^* = 0.08$, $\epsilon = -0.8$; **T2**: Tomographic, thermochemical, $E = 6.5\cdot10^{-3}$, $Pm = 20$, $Ra = 2.8\cdot10^4$, variable $\bar{q}^*, \delta q_c^* = 0.06$, $\epsilon = -0.8$; **T3**: Tomographic, thermochemical, $E = 6.5\cdot10^{-3}$, $Pm = 20$, $Ra = 2.8\cdot10^4$, $\bar{q}^* = 0$, variable $\delta q_c^*, \epsilon = -0.8$.

Type	Ra	δt^*	B_d^*	δB_d^*	N	Rm	Ro_ℓ
U1	$6\cdot10^4$	100	0.77	0.14	0	105	0.035
U1	$7\cdot10^4$	190	0.72	0.20	0	129	0.045
U1	$8\cdot10^4$	120	0.60	0.23	1	150	0.055
U1	$8.5\cdot10^4$	267	0.53	0.21	6	155	0.057
U1	$9\cdot10^4$	100	0.51	0.23	4	169	0.062
U1	$1\cdot10^5$	105	0.50	0.28	17	181	0.068
U1	$1.2\cdot10^5$	82	0.31	0.24	24	213	0.078
U1	$1.35\cdot10^5$	77	0.29	0.22	24	233	0.087
U1	$1.5\cdot10^5$	68	0.25	0.20	24	256	0.10
U1	$1.8\cdot10^5$	60	0.24	0.18	33	290	0.12
U1	$2\cdot10^5$	52	0.20	0.14	29	311	0.13
U2	$1.8\cdot10^4$	82	0.61	0.00	0	96	0.028
U2	$2\cdot10^4$	82	1.1	0.16	0	93	0.032
U2	$2.2\cdot10^4$	81	0.95	0.18	0	106	0.037
U2	$2.4\cdot10^4$	81	0.84	0.19	0	117	0.041
U2	$2.6\cdot10^4$	81	0.79	0.15	0	126	0.044
U2	$2.8\cdot10^4$	235	0.74	0.17	0	137	0.048
U2	$2.9\cdot10^4$	175	0.70	0.21	2	143	0.0505
U2	$3\cdot10^4$	235	0.58	0.23	5	151	0.053
U2	$4\cdot10^4$	146	0.47	0.32	18	191	0.069
U2	$5\cdot10^4$	115	0.29	0.24	28	235	0.087
U2	$6\cdot10^4$	98	0.29	0.26	40	269	0.105
U2	$7\cdot10^4$	90	0.20	0.16	39	300	0.122
Type	E	δt^*	B_d^*	δB_d^*	N	Rm	Ro_ℓ
U3	$4.5\cdot10^{-3}$	152	0.89	0.12	0	144	0.042
U3	$4.7\cdot10^{-3}$	152	0.78	0.18	0	153	0.047
U3	$5.2\cdot10^{-3}$	151	0.67	0.22	4	166	0.056
U3	$5.5\cdot10^{-3}$	151	0.58	0.22	2	174	0.062
U3	$5.8\cdot10^{-3}$	150	0.52	0.25	10	180	0.063
U3	$6.1\cdot10^{-3}$	149	0.50	0.27	16	182	0.067
U3	$6.5\cdot10^{-3}$	148	0.30	0.22	30	192	0.074
U3	$7.5\cdot10^{-3}$	50	0.21	0.16	21	209	0.086
Type	Ra	δt^*	B_d^*	δB_d^*	N	Rm	Ro_ℓ
U4	$3\cdot10^6$	400	0.357	0.08	0	184	0.035
U4	$7\cdot10^6$	278	0.193	0.09	5	375	0.075
UT	$1\cdot10^5$	80	0.92	0	0	39	0.013
UT	$1.5\cdot10^5$	80	0.99	0.07	0	61	0.022
UT	$2\cdot10^5$	80	0.77	0.11	0	83	0.031
UT	$2.5\cdot10^5$	80	0.66	0.1	0	106	0.046
UT	$3\cdot10^5$	80	0.51	0.1	0	137	0.063
UT	$3.5\cdot10^5$	80	0.3	0.1	0	170	0.089
UT	$4\cdot10^5$	80	0.04	0.01	0	200	0.11
UT	$4.5\cdot10^5$	80	0.05	0.02	0	225	0.13
T1	$1.5\cdot10^4$	60	0.92	0.05	0	79	0.030
T1	$2\cdot10^4$	60	0.84	0.16	0	104	0.038
T1	$2.5\cdot10^4$	60	0.70	0.23	2	134	0.048
T1	$3\cdot10^4$	272.5	0.58	0.28	20	166	0.058
T1	$3.5\cdot10^4$	60	0.50	0.26	6	187	0.067
T1	$4\cdot10^4$	60	0.42	0.27	9	208	0.076
T1	$4.5\cdot10^4$	60	0.31	0.24	15	230	0.085
T1	$5\cdot10^4$	52	0.26	0.20	19	251	0.094
T1	$5.5\cdot104$	49	0.22	0.17	22	271	0.104
T1	$6\cdot10^4$	45	0.22	0.16	23	286	0.113
Type	$\bar{q}^*$	δt^*	B_d^*	δB_d^*	N	Rm	Ro_ℓ
T2	−0.12	265	0.67	0.084	0	111	0.044
T2	−0.06	400	0.59	0.16	10	134	0.053
T2	0.00	343	0.48	0.25	30	157	0.061
T2	+0.06	85	0.39	0.22	13	173	0.070
Type	δq_c^*	δt^*	B_d^*	δB_d^*	N	Rm	Ro_ℓ
T3	0	267	0.53	0.21	6	155	0.057
T3	0.06	262	0.48	0.25	23	157	0.060
T3	0.08	80	0.52	0.26	6	159	0.061
T3	0.12	40	0.36	0.21	7	166	0.066
T3	0.16	40	0.23	0.21	8	172	0.070
T3	0.24	35	0.21	0.20	10	166	0.078

Table 2
Reversal statistics from chemical dynamos with $E = 6.5 \cdot 10^{-3}$, $Pm = 20$, $Ra = 2.8 \cdot 10^4$, $\bar{q}^* = 0$, variable δq_c^* and $\epsilon = -1$ from Olson et al. (2010).

Y-Type	δq_c^*	δt^*	B_d^*	δB_d^*	N	Rm	Ro_ℓ
$+Y22$	0.06	130	0.469	0.283	4	158	0.061
$Y2211$	0.045	119	0.591	0.307	8	155	0.060
$-Y20$	0.045	40	0.210	0.125	3	170	0.068
$Y11$	0.060	165	0.509	0.234	18	155	0.060
$Y40$	0.045	40	0.519	0.242	5	153	0.059
$Y20$	0.045	40	0.337	0.208	19	154	0.057
$Y10$	0.045	120	0.536	0.307	8	156	0.056

Table 3
Reversal statistics from chemical dynamos with imposed Y_2^0 CMB heat flux pattern, $E = 1.5 \cdot 10^{-3}$, $Pm = 20$, variable Ra, $\bar{q}^* = 0$, $\delta q_c^* = 0.3$ and $\epsilon = -1$. $+Y20/-Y20$ correspond to positive heat flux anomaly at the equator/pole (equatorial/polar cooling), respectively.

Y-Type	Ra	δt^*	B_d^*	δB_d^*	N	Rm	Ro_ℓ
$+Y20$	20000	36	1.1	0.16	0	289	0.036
$+Y20$	25000	26	0.98	0.23	0	342	0.045
$+Y20$	30000	22	0.52	0.30	2	422	0.059
$-Y20$	20000	31	0.71	0.11	0	289	0.036
$-Y20$	25000	26	0.65	0.12	0	389	0.051
$-Y20$	30000	24	0.27	0.21	6	456	0.074

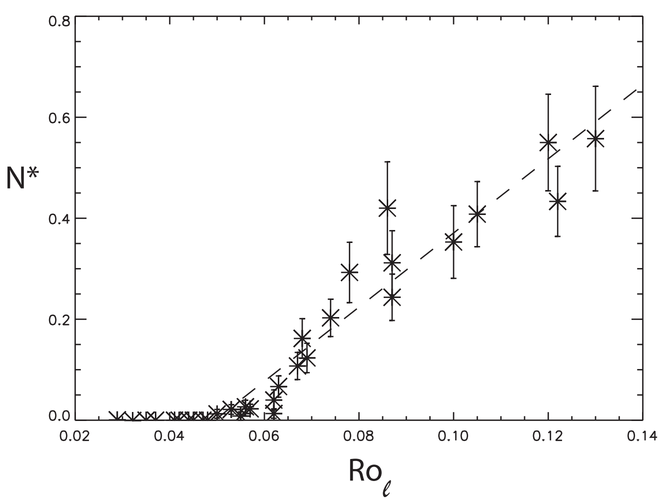

Fig. 1. Dimensionless reversal frequency versus local Rossby number for dynamos with uniform CMB heat flux. Dashed line is the fit from Table 4.

Table 4
Summary of least squares fits to $N^* = a \cdot Ro_\ell + b$ for $N^* > 0$, where Ro_ℓ is the local Rossby number. Ro'_ℓ is the local Rossby number corrected for boundary heterogeneity. Margins of errors to linear fit coefficients are given in $\pm$. The intercept of the linear fits with the x-axis $-b/a$ gives the critical value $Ro_{\ell crit}$ for the onset of reversals. U and T denote uniform and tomographic CMB heat flux dynamos, respectively. The number of reversing dynamo models is N_{cases}. Ra and E denote cases with variable Rayleigh and Ekman numbers respectively, $\bar{q}$ and δq denote cases with variable mean and laterally heterogeneous CMB heat flux respectively. The last entry is the fit to $\sigma^* = a \cdot Ro_\ell + b$.

Type (variables)	N_{cases}	a	b	$Ro_{\ell crit}$
$U(Ra, E)$ vs. Ro_ℓ	22	7.39 ± 0.51	-0.38 ± 0.05	0.0504 ± 0.006
$T(Ra, E)$ vs. Ro_ℓ	12	7.61 ± 0.45	-0.37 ± 0.03	0.0482 ± 0.004
$T(Ra, E)$ vs. Ro'_ℓ	12	7.31 ± 0.45	-0.37 ± 0.03	0.0501 ± 0.004
$T(\bar{q})$ vs. Ro_ℓ	3	7.52 ± 0.15	-0.37 ± 0.02	0.0496 ± 0.003
$T(\delta q)$ vs. Ro_ℓ	6	12.3 ± 1.0	-0.66 ± 0.07	0.0537 ± 0.006
$T(\delta q)$ vs. Ro'_ℓ	5	8.19 ± 0.9	-0.42 ± 0.08	0.0515 ± 0.006
σ^* vs. Ro_ℓ	42	14.3 ± 1.1	-0.43 ± 0.09	0.030 ± 0.006

Tables 1–3 give time averages of the global magnetic Reynolds number Rm and the local Rossby number Ro_ℓ as defined by (14) and (17). The first column denotes the type of patterns imposed on the outer boundary of the thermochemical dynamos, including uniform (U), tomographic (T), and single spherical harmonic (Y) CMB heat fluxes respectively. For the T-type dynamos, the boundary heat flux heterogeneity pattern is the same as used in Olson et al. (2013) and the heterogeneity amplitude is given in terms of (9). Dynamos labeled $\pm$Y20 use CMB heat flux heterogeneity described by a single spherical harmonic of degree 2 and order 0 (Table 3). The cumulative duration of all the thermochemical dynamos in Tables 1–3 is about $8750\tau_d$, and the cumulative number of reversals is about 800.

3.1. Uniform CMB heat flux

Fig. 1 shows N^* versus Ro_ℓ from the dynamos labeled U1-U3 in Table 1 with homogeneous CMB conditions for various Ra, $\bar{q}^*$ and E. The error bars correspond to (12). Stable polarity is found in all cases with $Ro_\ell < 0.045$ and reversing polarity in all cases with $Ro_\ell \geqslant 0.051$ approximately. The frequency of reversals tends to increase with increasing Ro_ℓ. The dashed line in Fig. 1 is a linear fit to all of the reversing cases, and as shown in Table 4, is given by $N^* = 7.39 Ro_\ell - 0.38$. The intercept value, which we use to estimate the critical value of the local Rossby number defining reversal onset, is given by $Ro_{\ell crit} = 0.0504$. There is a suggestion in Fig. 1 that the transition from fixed to reversing polarity may not be linear, and in addition, the variation of N^* at supercritical Ro_ℓ has substantial scatter. Nevertheless, we were unable to resolve significant nonlinear trends in the data beyond $Ro_{\ell crit}$, and the statistics of the fit bear this out; the errors are only $\sim 10\%$ of the linear fit coefficients in Table 4.

The cases labeled UT in Table 1 are driven by thermal convection with fixed temperature boundary conditions, no internal heat sources or sinks, and smaller E and Pm. These were included for comparison with the thermochemical dynamos. Previous studies (Christensen and Aubert, 2006; Olson and Christensen, 2006) have shown that reversing dipolar-type dynamos with isothermal boundary conditions are concentrated in an extremely narrow range of Ro_ℓ, and are therefore ill-suited for the type of scaling analysis we perform in this paper. Our UT cases also show this, and point to the importance of buoyancy distribution and boundary conditions in governing reversal behavior. No reversals were

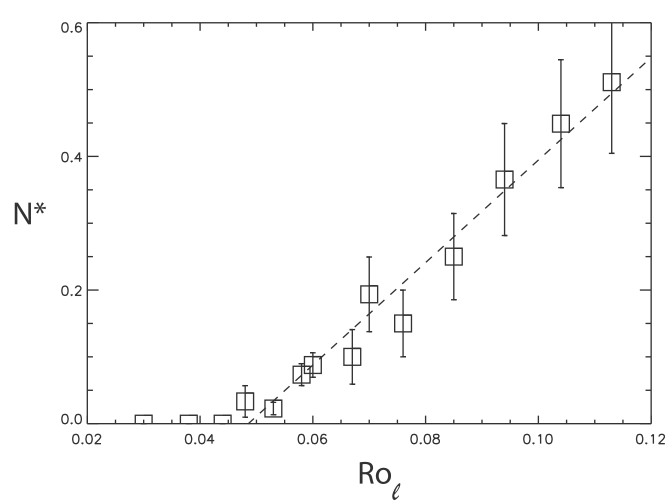

Fig. 2. Dimensionless reversal frequency versus local Rossby number for dynamos with tomographic CMB heat flux and heterogeneity amplitude $\delta q_c^* = 0.08$. Dashed line is the fit from Table 4.

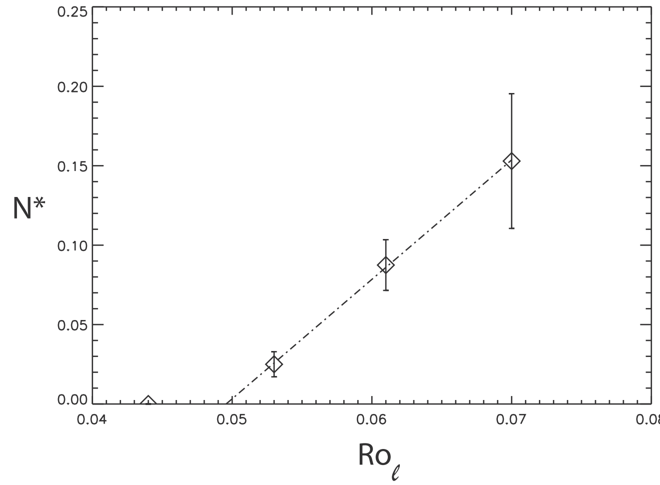

Fig. 3. Dimensionless reversal frequency versus local Rossby number for dynamos with fixed tomographic CMB heat flux heterogeneity and various mean CMB heat fluxes $\bar{q}^*$. Dashed line is the fit from Table 4.

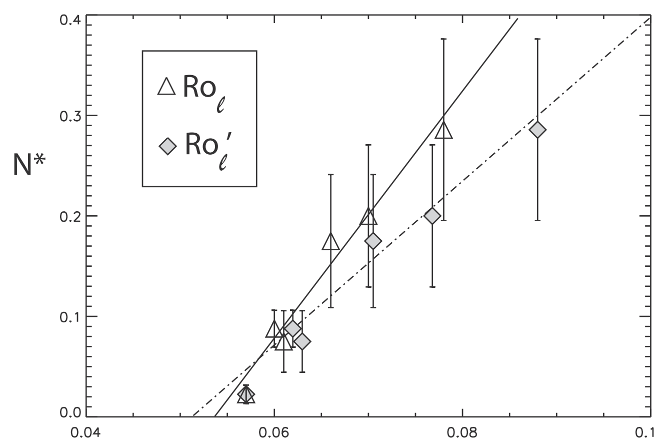

Fig. 4. Dimensionless reversal frequency versus local Rossby number for dynamos with tomographic CMB heat flux pattern and various heterogeneity amplitudes δq_c^*. Triangles are uncorrected Ro_ℓ, diamonds are corrected using $Ro'_\ell = Ro_\ell(1 + \delta q_c^*/2)$. Solid and dashed-dot lines are the fits to the uncorrected and corrected data, respectively, from Table 4.

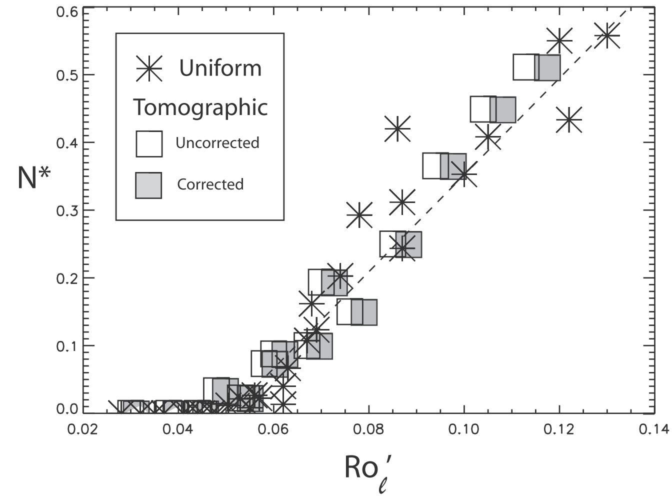

Fig. 5. Dimensionless reversal frequency versus corrected local Rossby number for boundary heterogeneity from dynamos with uniform and tomographic boundary conditions. Dashed line is the fit to the corrected values from Table 4. Open symbols are tomographic dynamos with uncorrected local Rossby number.

recorded in our UT dynamos, even though their magnetic Reynolds numbers and local Rossby numbers spanned broad ranges, $39 \leqslant Rm \leqslant 225$ and $0.013 \leqslant Ro_\ell \leqslant 0.13$, respectively.

3.2. Tomographic CMB heat flux, variable control parameters

Fig. 2 shows N^* versus Ro_ℓ for the dynamos labeled T1 in Table 1 with tomographic CMB conditions and variable Ra. The definition of the error bars are the same as in Fig. 1. Like the U-type dynamos, these tomographic dynamos have fixed polarity for small Ro_ℓ and reversal frequency increasing generally linearly at higher Ro_ℓ. The dashed line in Fig. 2 is again a linear fit to all of the reversing cases, and is given by $N^* = 7.61Ro_\ell - 0.37$, as shown in Table 4. The intercept value for the T1 dynamos is given by $Ro_{\ell crit} = 0.0482$, somewhat smaller than for the U-type dynamos. The slight reduction in $Ro_{\ell crit}$ in these tomographic dynamos is consistent with the general tendency for increase in reversal frequency in dynamos with boundary heterogeneity compared to otherwise similar dynamos with uniform boundary conditions (Olson et al., 2010).

Fig. 3 shows N^* versus Ro_ℓ for the dynamos labeled T2 in Table 1 with tomographic CMB conditions and variable average CMB heat flux represented by variable $\bar{q}^*$. Consistent with cases U1–U3 and T1, Fig. 3 shows fixed polarity for small Ro_ℓ and a regularly linear increase in reversal frequency at higher Ro_ℓ. The dashed-dot line in Fig. 3 is again a linear fit to the reversing cases, and yields $N^* = 7.52Ro_\ell - 0.37$. The intercept of this fit yields $Ro_{\ell crit} = 0.0496$, a value intermediate between the T1 and U-type dynamos.

We conclude from the results in Figs. 1–3 that the average reversal frequency in these thermochemical dynamos can be expressed in terms of the local Rossby number, with the transition from fixed to reversing polarity around $Ro_{\ell crit} \simeq 0.05$ approximately, and with a sensitivity in the reversing regime given approximately by

$$N^* = aRo_\ell + b \qquad (18)$$

with $a \simeq 7.5$ and $b \simeq -0.4$.

3.3. Heterogeneous CMB heat flux, variable boundary heterogeneity

Fig. 4 shows N^* versus Ro_ℓ for the dynamos labeled T3 in Table 1 with tomographic CMB conditions and variable amplitude of the tomographic heterogeneity, represented by δq_c^*. The open triangles correspond to the Ro_ℓ-values from Table 1. For these dynamos, N^* tends to increase with Ro_ℓ at a rate that is substantially higher than in Figs. 1–3. Fitting the data in Fig. 4 to (18) yields $a \simeq 12.3$ and $b \simeq -0.66$, significantly different from the previous cases. A plausible explanation for the discrepancy is that Ro_ℓ, which is a local measure of the convective vigor, becomes increasingly spatially heterogeneous with increasing δq_c^*, so that Ro_ℓ is anomalously large in the outer core beneath regions where the CMB heat flux heterogeneity $q'(\phi, \theta)$ is positive, and Ro_ℓ is anomalously small beneath regions where q' is negative.

If we assume that dynamo reversals are initiated locally (as previous studies indicate), then the difference between N^* versus Ro_ℓ in Fig. 4 compared to Figs. 1–3 can be lessened by replacing Ro_ℓ with its value based on contributions beneath the regions of highest CMB heat flux. Accordingly, we define a heterogeneity-corrected local Rossby number

$$Ro'_\ell = Ro_\ell(1 + \delta q_c^*/2) \qquad (19)$$

The 1/2-factor appearing in (19) represents the first term in a Taylor expansion of the scaling laws used in the next section, which indicate that Ro_ℓ varies approximately as the square root

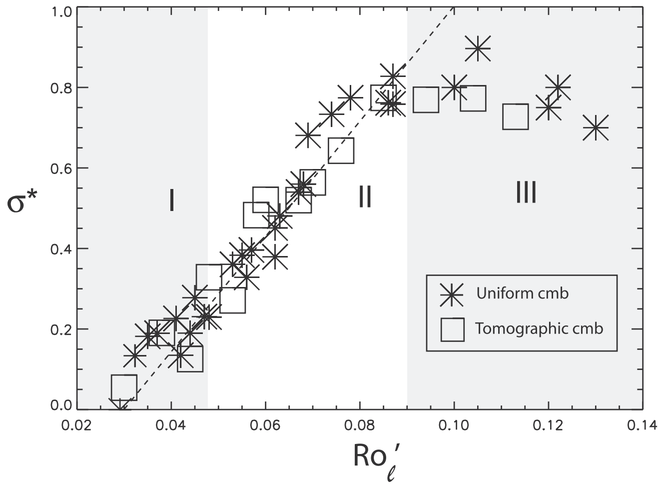

Fig. 6. Relative standard deviation of dipole fluctuations versus corrected local Rossby number for dynamos with uniform and tomographic CMB heat flux. Shaded areas I,II, and III denote non-reversing, linear reversing, and saturated reversing regions, respectively. Dashed line is the fit from Table 4.

of the CMB heat flux (Aubert et al., 2009). The filled diamond symbols in Fig. 4 correspond to replacement of Ro_ℓ for the T3 dynamos in Table 1 by Ro'_ℓ, and the dashed-dot line corresponds to the least squares fit of (18) to the corrected points. As the coefficients of the fit in Table 4 reveal, using Ro'_ℓ brings the reversal frequencies for variable CMB heterogeneity amplitude into closer agreement with results from the U-type dynamos. As a demonstration that the corrected local Rossby number concept works more generally, we show in Fig. 5 N^* versus Ro'_ℓ for U and T1-type dynamos. The two dynamo types collapse nicely onto the same trend, the parameters of which are given in Table 4. In particular, we obtain $Ro^*_{\ell crit} = 0.0501$ for the critical local Rossby number corrected for the amplitude of the tomographic boundary heterogeneity.

However, this amplitude-based correction may not work so well when comparing cases with different planforms of boundary heterogeneity. Table 2 shows results obtained by Olson et al. (2010) for various patterns of CMB heat flux heterogeneity, mostly consisting of a single spherical harmonic, except for one case ($Y2211$) that is a superposition of two spherical harmonics. Although these cases have comparable Ro'_ℓ-values, nevertheless

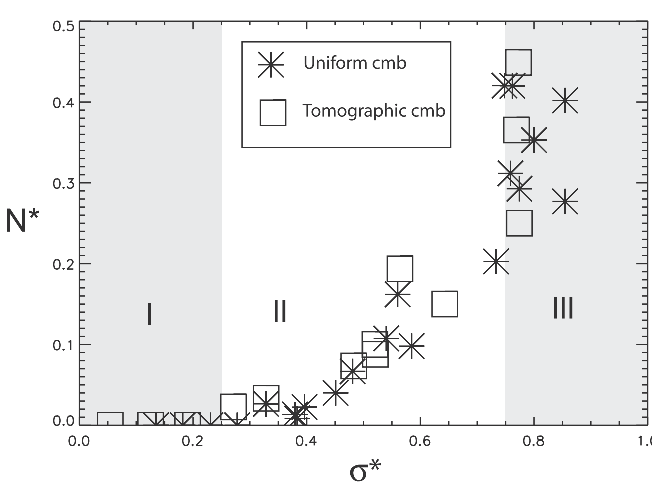

Fig. 7. Dimensionless reversal frequency versus the relative standard deviation of dipole fluctuations for dynamos with uniform and tomographic CMB heat flux. Shaded areas I,II, and III denote non-reversing, linear reversing, and saturated reversing regions, respectively.

there is a large difference in reversal frequency between the $+Y20$ case and the others. In particular, $N^* = 0.47$ for the $+Y20$ case, whereas $N^* = 0.075$ for the $-Y20$ case. Extreme reversal sensitivity in dynamos with zonal heat flux heterogeneity has been reported previously (Glatzmaier et al., 1999; Kutzner and Christensen, 2004), generally with higher reversal rates in $+Y20$ cases, corresponding to elevated heat flux near the equator. Yet the behavior of the $\pm Y20$ cases in Table 3 are inconsistent with this rule, suggesting that multiple factors may control reversal behavior in dynamos with zonal heterogeneity. We consider the effects of zonal heterogeneity separately in a later section.

3.4. Dipole moment fluctuations

Fig. 6 shows the relative standard deviation of the dipole intensity σ^* versus Ro_ℓ for all of the U-type and T-type dynamos in Table 1. Three regions can be defined. In region I the relation is linear with a positive slope, but this region corresponds to subcritical Ro_ℓ-values, that is, non-reversing dynamo states. In region II the relation is again linear with a positive slope similar to that of region I, and in addition, Ro_ℓ is supercritical for reversals. The dashed line shows the best linear fit to the relation in regions I and II, with parameters given in Table 4. It applies to $Ro_\ell \leqslant 0.09$, which according to Figs. 1–4, covers most of the reversal frequency range represented in the paleomagnetic record. However, in region III of Fig. 6 the linear correlation degrades and σ^* saturates. According to Table 1, most of the dynamos in region III have relatively weak dipole fields or are of the multipolar type, and therefore are less representative of the paleomagnetic field than the dynamos in regions I and II.

Fig. 7 shows the reversal frequency N^* versus the relative standard deviation of the dipole intensity σ^*, divided into the same three regions as in Fig. 6. There is a positive correlation between these two parameters in region II, although the scatter is somewhat larger than in the same region of Fig. 6. A linear fit of N^* to σ^* could be made in region II, but with such large uncertainty that it may not be of much use in practice. Instead, it may be more useful to refer to the limits of region II. According to Fig. 7, $\sigma^*_{crit} \simeq 0.25$ at reversal onset ($N^* \simeq 0$), and $\sigma^*_{crit} \simeq 0.75$ for frequently reversing conditions, for which $N^* > 0.25$.

4. Application to the Geodynamo

4.1. Reversal frequency versus core heat flux

In this section we apply numerical dynamo scaling relationships to relate variations in Ro_ℓ to variations in Q_{cmb}, the total heat flux from the core, for a range of values of outer core transport

Table 5
Dimensionless parameters in (20) for each choice of thermal conductivity (in W/m/K) used for obtaining Fig. 8. The ranges of Q_{cmb} considered are also given. $Q_{cmb\,crit}$ is the CMB heat flux at $Ro_{\ell crit}$; $Q_{cmb\,ad}$ is the CMB adiabatic heat flux.

Parameter	$k = 70$	$k = 100$	$k = 130$
Q_{cmb} (TW)	5.5–10	8–13	10–15
Pr	2.7	1.9	1.4
Pm	$1.7{\cdot}10^{-5}$	$2.4 \cdot 10^{-5}$	$3.1 \cdot 10^{-5}$
E	$5.4{\cdot}10^{-14}$	$5.4 \cdot 10^{-14}$	$5.4 \cdot 10^{-14}$
γ	0.6–0.4	0.6–0.4	0.6–0.4
τ_d (kyr)	33	47.5	62
N^*, 0–5 Ma	0.13	0.19	0.25
Ro_ℓ $(\delta q^* = 0)$, 0–5 Ma	0.07	0.079	0.087
δq^* $(Ro_\ell = Ro_{\ell crit})$, 0–5 Ma	0.8	1.16	1.48
Q_{cmb}, 0–5 Ma (TW)	7.4	11	15
$Q_{cmb\,crit}$ (TW)	6.3	8.7	11.4
$Q_{cmb\,ad}$ (TW)	8.3	11.9	15.4

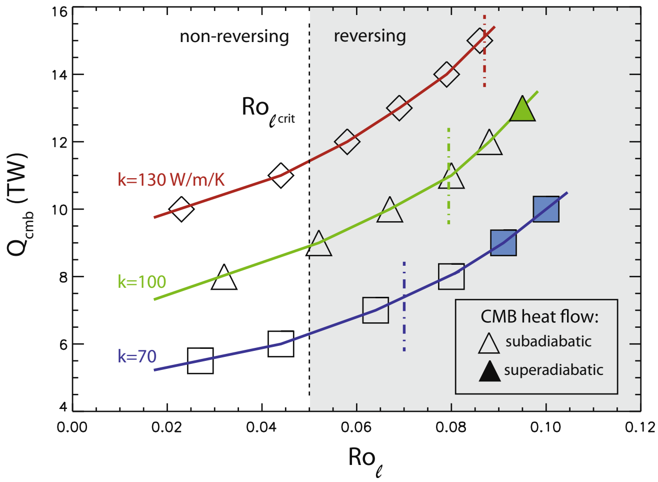

Fig. 8. Total core–mantle boundary heat flux in terawatts (TW) versus local Rossby number for three values of the thermal conductivity of the core, calculated using the parameters in Table 5 and the scaling law (20). Open and filled symbols indicate thermally subadiabatic and superadiabatic outer core stratification, respectively. Vertical dashed-dot and short dashed lines denote estimated present-day local Rossby number (color coded for each *k*-value) and the critical local Rossby number (in black), respectively. Shaded and unshaded regions indicate reversing and non-reversing dynamo regimes.

properties. We start with the scaling law for Ro_ℓ for convective dynamos obtained by Aubert et al. (2009):

$$Ro_\ell/(1+r_i/r_o) = 0.54E^{-0.32}Pr^{0.19}Pm^{-0.19}(\gamma Ra_Q)^{0.48} \tag{20}$$

where γ is defined in Eq. (18) of Aubert et al. (2009) in terms of r_i, r_o and the buoyancy distribution in the outer core, and

$$Ra_Q = \frac{g(F_o+F_i)}{4\pi\rho\Omega^3 D^4}, \tag{21}$$

where F_o and F_i are the buoyancy production (in kg/s) at the outer and inner boundaries of the outer core, respectively. To calculate F_o and F_i, we use a standard model of the buoyancy profile in the outer core (Labrosse, 2003; Olson et al., 2013) that includes inner core growth but zero radioactive heat production, for a range of plausible core heat flux values Q_{cmb}. We consider high, medium, and low values of the thermal conductivity of the core, corresponding to k = 130, 100, and 70 $W/m/K$, respectively, with electrical conductivity σ based on the Wiedemann–Franz law

$$k = L\sigma T \tag{22}$$

with $L = 2.45\times10^{-8}$ $W/S/K^2$ and $T = 4200$ K. We assume $\nu = 2\times10^{-5}$ m^2/s for the outer core viscosity. Table 5 gives values for the dimensionless parameters that appear in (20) for each choice of thermal conductivity. The values of Q_{cmb} considered are also given in Table 5.

Fig. 8 shows the results of these calculations, with Q_{cmb} expressed as a function of Ro_ℓ. Q_{cmb} increases non-linearly with Ro_ℓ and increases approximately linearly with k. It is remarkable that only moderate changes in Q_{cmb} are needed to produce substantial changes in Ro_ℓ, which means that only moderate core heat flux changes are needed to produce large changes in geomagnetic reversal frequency. As examples, Table 5 gives the dipole free decay time τ_d, the corresponding present-day (0–5 Ma) value of N^* based on $N = 4$/Myr, and the present-day (0–5 Ma) value of Ro_ℓ in the core based on (18), for each thermal conductivity choice. The 0–5 Ma Ro_ℓ-values are shown by vertical dashed-dot lines in Fig. 8, and yield $Q_{cmb} = 7.4$ TW (low conductivity), 11 TW (intermediate conductivity), or 15 TW (high conductivity) for the total core heat flux consistent with the present-day (0–5 Ma) geomagnetic reversal rate.

The unshaded and shaded backgrounds in Fig. 8 denote non-reversing and reversing dynamo regimes, based on $Ro_{\ell crit}$ = 0.05. The curves in Fig. 8 intersect this boundary at core heat fluxes of $Q_{cmb} = 6.3$ TW (low conductivity), 8.7 TW (intermediate conductivity) or 11.4 TW (high conductivity). Assuming that $Ro_{\ell crit}$ defines the onset of superchron behavior, then the change in core heat flux needed to produce a superchron, starting from present-day core conditions, corresponds to $\delta Q_{cmb} = -1.1$ TW (low conductivity), -2.3 TW (intermediate conductivity), or -3.6 TW (high conductivity).

The above calculations give the required changes in CMB heat flux *magnitude* (with homogeneous pattern) in order for the geodynamo to turn from present day conditions to a superchron. Alternatively, a reduction in reversal frequency may occur due to reduction in CMB heat flux heterogeneity alone. Assuming a critical local Rossby number for the onset of reversals of $Ro'_\ell = Ro_{\ell crit} = 0.05$, we apply (19) to calculate the amplitude of CMB heat flux heterogeneity required to obtain the same Ro'_ℓ values as the values of Ro_ℓ for the U-type dynamos. We obtain δq^*-values (Table 5) of 0.8 (low conductivity), 1.16 (intermediate conductivity), or 1.48 (high conductivity). These values represent the required reductions in the non-dimensional heat flux heterogeneity amplitude in order to turn from present-day reversal frequency to a superchron.

The relation between the CMB heat flux and the local Rossby number (Fig. 8), our scaling law (18) and the heteogeneity-correction (19) define several possible connections between the observed variations in paleomagnetic reversal frequency during the Phanerzoic and time variations in mantle convection. For example, during the Creteceaus Normal Superchron, subcritical conditions could have been caused by reduced total CMB heat flux, reduced CMB heat flux heterogeneity, or a combination of these two. Unfortunately, results from mantle general circulation models (MGCMs) typically show higher than average Q_{cmb} with little change in q' during the Cretaceous Normal Superchron (Zhang and Zhong, 2011; Olson et al., 2013). However, the CMB heat flux predicted by MGCMs during the Cretaceous remains uncertain because of uncertainty in key mantle properties, including the density and viscosity stratification in the transition zone and in the D″ layer, the radioactive heat content of the lower mantle, as well as the plate reconstructions that are used as surface boundary conditions.

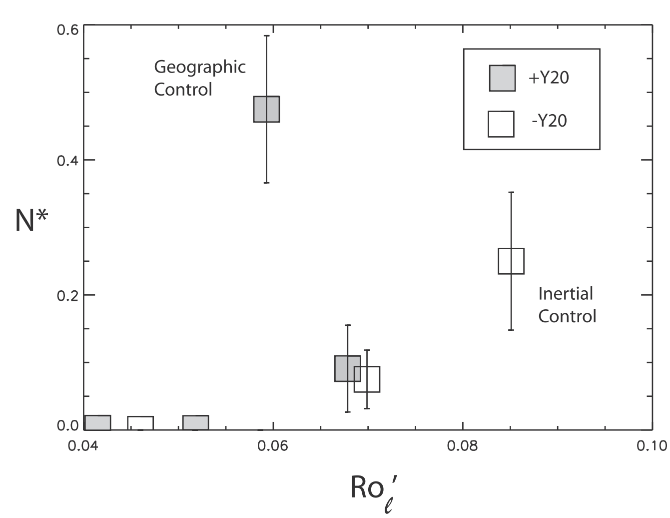

Fig. 9. Dimensionless reversal frequency versus corrected local Rossby number for dynamos with $\pm Y20$ CMB heat flux patterns.

4.2. Reversal frequency versus dipole moment fluctuations

Although the local Rossby number correlates with reversal frequency in numerical dynamos, application to the geodynamo is limited by the fact that Ro_ℓ depends on the convective length scale, which is expected to be too small to be seen in the geomagnetic field structure or its secular variation (Holme, 2007; Finlay and Amit, 2011). There are some indirect methods for estimating Ro_ℓ, but they yield disparate results. For example, Finlay and Amit (2011) inferred ℓ_u from maxima of SV spectra extrapolated from observed geomagnetic field models. Combined with their estimates for the magnitude of the small-scale core flow, they obtained Ro_ℓ values about two orders of magnitude smaller than estimates of global Ro. However, their local Rossby number is still two orders of magnitude larger than that inferred from the numerical dynamos in this study and others (Christensen and Aubert, 2006; Olson and Christensen, 2006), and is very far from the critical value we infer for the onset of reversals. Accordingly, there is a need to establish a more direct, observable proxy for Ro_ℓ in the core.

As a proxy for Ro_ℓ, we have shown that the relative standard deviation of the dipole moment correlates with reversal frequency, although the correlation in this case involves more scatter and is not everywhere linear, particularly in region III in Figs. 6 and 7. For $Ro_\ell > 0.1$, the reversal frequency continues to grow approximately linearly with Ro_ℓ, but in this regime the field looses its dipole dominance and there is no clear-cut difference between the stability of the dipole and the other field harmonics. Nevertheless, it is interesting to compare the predictions of our numerical dynamos with paleomagnetic data in terms of these parameters. From Table 5, $N^* \simeq 0.13 - 0.25$ would apply to the 0–5 Ma paleomagnetic field, which corresponds to $\sigma^* \simeq 0.5 - 0.75$ according to Fig. 7. For comparison, fluctuations in the virtual dipole intensity for the 0–2 Ma paleomagnetic field yield $\sigma^* \simeq 0.32$ according to the SINT2000 (Valet et al., 2005) and the PADM2M (Ziegler et al., 2011) reconstructions. The σ^*-values predicted from our numerical dynamos exceed those inferred from reconstructions of the paleomagnetic field intensity by about a factor of two. However, those reconstructions are based on virtual dipole intensity, and as a consequence they underestimate the true dipole intensity fluctuations by not properly accounting for the non-dipole field, and in addition, they likely smooth the higher frequency intensity fluctuations in our numerical dynamos.

To examine whether the differences in the dipole variability in our models compared to SINT2000 are due to differences in sampling and smoothing, we have recalculated σ^* in our models by downsampling the dipole intensity timeseries. Using smoothing intervals of 1 kyr (comparable to those reported for SINT2000) we obtain negligible reductions. For our reversing dynamos, to reproduce the SINT2000 σ^* we need to downsample at intervals of about one dipole decay time, far larger than 1 kyr. From these tests we infer that smoothing is not the reason for our larger σ^*-values. Instead, there appears to be either more dipole variability or less non-dipole variability in our dynamo models compared to SINT2000.

5. Geographic versus inertial control

There are several unresolved issues concerning the effects on reversals of zonal patterns of boundary heterogeneity. In the Introduction we summarize previous studies that have proposed explanations for reversal sensitivity in dynamos with diverse patterns of CMB heat flux heterogeneity. The overall effect of boundary heterogeneity as reported in these studies is an increase in reversal sensitivity, consistent with our interpretation that the heterogeneity produces local maxima in Ro_ℓ, thus promoting reversals. However, some previous studies (Glatzmaier et al., 1999; Kutzner and Christensen, 2004) report enhanced polarity stability with certain boundary heterogeneity patterns, most notably, patterns that include zonal spherical harmonics such as $-Y20$, the negative sign indicating reduced CMB heat flux in the equatorial region and enhanced CMB heat flux in the polar regions.

We have explored this effect in our dynamos, comparing polarity stability with $\pm Y20$-type boundary heterogeneity, the $+$ sign indicating enhanced equatorial heat flux (i.e., equatorial cooling), the $-$ sign indicating reduced equatorial heat flux. Fig. 9 shows the reversal frequency of dynamos with positive and negative $Y20$ CMB heterogeneity for the parameters in Table 3 (this study) and Table 2 (Olson et al., 2010). Lower Ekman numbers were used for these cases to make them more similar to the previous studies (Glatzmaier et al., 1999; Kutzner and Christensen, 2004). Each pair of $\pm Y20$ reversing cases has the same control parameters and CMB heat flux heterogeneity amplitude, so the two cases in each pair differ only by the sign of the pattern. Fig. 9 contains two pairs of $\pm Y20$ reversing cases. For each pair the $-Y20$ cases yield larger Ro'_ℓ. However, in the pair with the lower Ro'_ℓ values, the $+Y20$ case reverses more often, whereas in the pair with the larger Ro'_ℓ the $-Y20$ case reverses more often. We explain this behavior in terms of boundary pattern compatibility with the underlying compositionally-driven convection, modified by a competition between an additional geographic effect and an inertial effect.

The larger Ro'_ℓ values in the $-Y20$ cases can readily be explained in terms of boundary pattern compatibility with the underlying convection. The time average zonal flow and meridional circulation in numerical dynamos with uniform CMB conditions is characterized by an equatorial upwelling and high-latitude downwellings (e.g. Aubert, 2005; Amit and Olson, 2006). This is similar to the flow driven by a $-Y20$ boundary heterogeneity. Accordingly, compatibility with $-Y20$-type boundary heterogeneity enhances the compositionally-driven convection and increases the local Rossby number, whereas incompatibility with $+Y20$-type boundary heterogeneity weakens the convection and decreases the local Rossby number.

However, the reversal frequencies in Fig. 9 require modifications to this explanation. First, the $+Y20$ case in Table 2 reverses more than its $-Y20$ counterpart because equatorial cooling strengthens the equatorial downwelling and concentrates low-latitude magnetic flux in the $+Y20$ case, thereby increasing its likelihood of reversing. We use the term *geographic control* for this effect. Second, the $-Y20$ case in Table 3 reverses more than its $+Y20$ counterpart because the $-Y20$ case features smaller convective length scales due to the compatibility of the -Y20 boundary driven flow with the underlying convection. We use the term *inertial control* for this effect.

Competing geographic and inertial effects offer a resolution of the ambiguities in previous studies of reversals with zonal boundary heterogeneity. $+Y_2^0$ pattern increases in reversal frequency (Glatzmaier et al., 1999; Kutzner and Christensen, 2004; Olson et al., 2010) may result from low-latitude magnetic flux concentration enhancing the dipole axis tilt (Amit et al., 2010). Likewise, Glatzmaier et al. (1999) and Kutzner and Christensen (2004) found superchron-type behavior for $-Y_2^0$, which may be interpreted as dipole stability due to the repulsion of magnetic flux from low-latitudes. However, Olson et al. (2010) obtained larger reversal frequency for $-Y_2^0$ than for their reference uniform case. The reason could be that the dynamo models of Glatzmaier et al. (1999) and Kutzner and Christensen (2004) were close enough to the transition from stable to reversing and with small enough δq^* where geographic control holds, whereas the models of Olson et al. (2010) are farther from the transition, so for those, inertial control is more important. It should be noted that the transition from stable to reversing dynamos is sharper for smaller E (Wicht et al., 2009), so it is probably more difficult to pin-point this transition with the large E models of Olson et al. (2010).

Another ambiguity that may be reconciled using the concept of the competing geographic and inertial effects is the dependence on δq^* in the study of Kutzner and Christensen (2004). They found for Y_2^2 and a low δq^* lower reversal frequency than in their reference uniform case, which may be interpreted as a stabilizing impact of the Y_2^2 pattern. However, increasing δq^* resulted in larger reversal frequencies than in the uniform case. We interpret this result as a transition from a stabilizing geographic effect in the small δq^* case to a destabilizing inertial effect in the large δq^* case. We note that boundary compatibility with underlying convection was previously invoked as a determining factor of reversal frequency by Glatzmaier et al. (1999). However, they argued that their $+Y20$ case reverses frequently because it is compatible with the underlying dynamo convection. In contrast, we argue that for low Ro'_ℓ in which the geographic control applies $+Y20$ may reverse frequently because of magnetic flux concentration by fluid downwelling at the equator despite the incompatibility of this CMB heat flux pattern with the underlying dynamo convection.

6. Planetary dynamo reversals in the deep past

How do our results bear on the question of reversals in the deep past, for the Earth and for other terrestrial planets that once had active dynamos, such as Mars? Evidence of geomagnetic reversals have been found well into the Archaen (Layer et al., 1996), and there is evidence of both superchrons and hyper-reversing states in the Precambrian (Pavlov and Gallet, 2010). Although the age of the inner core remains uncertain, thermal history calculations (Nimmo, 2007) generally indicate that the inner core nucleated within about 1 Ga, making it likely that geomagnetic reversals occurred well before the inner core contributed to the geodynamo.

Sources of buoyancy for convection in the Earth's core prior to inner core nucleation include secular cooling, radiogenic heat production, and more speculatively, segregation of insoluble light elements from the outer core. As demonstrated by Hori et al. (2010), these buoyancy sources can be represented in numerical dynamos by a volumetric source term, as opposed to the volumetric sink term used for compositional convection in our study. In spite of this difference, however, dynamos powered by volumetric sources yield dipole-dominated fields that occasionally reverse in the same range of local Rossby numbers observed in this study (Aubert et al., 2009), provided that flux conditions are prescribed at the CMB (Hori et al., 2010). Furthermore, reversals are not seen in these dynamos when the local Rossby number is very small, and non-dipole fields result when the local Rossby number is large (Heimpel and Evans, 2013), qualitatively the same behavior as the dynamos in our study.

For the early dynamo on Mars, if we assume that it was powered by core convection, the buoyancy sources were probably similar to those just described for the early geodynamo, i.e., volumetric sources. Considerations of the thermal regime of the early Mars core indicate a substantial local Rossby number, approximately $Ro_\ell = 0.1$ (Olson and Christensen, 2006), which places the early Mars dynamo somewhere between regimes II and III in Figs. 6 and 7, implying that its dynamo may have been of the reversing type. Reversing dynamo calculations using a volumetric buoyancy source instead of a sink and without a solid inner core would be needed to substantiate this possibility.

Additional arguments favoring reversals of the ancient Martian field come from numerical dynamos driven by internal heating which aim at reproducing the hemispheric dichotomy observed in Mars' crustal magnetic field. Landeau and Aubert (2011) showed that an equatorially antisymmetric, axisymmetric convection mode arises spontaneously when convective vigor is increased. In the hemispherical dynamos obtained under such conditions, reversal likelihood is high. Amit et al. (2011) reported that the regime of non-reversing dynamos is more limited with internal heating dynamos than with other convection styles. Imposing an axial degree-1 CMB heat flux boundary condition, which is very effective in reproducing a magnetic hemispheric dichotomy (Stanley et al., 2008; Amit et al., 2011), may also result in increased reversal frequency (Dietrich and Wicht, 2013).

Finally, our results derived from Boussinesq dynamos may also be applicable to planetary dynamos in which compression is important, e.g. the gas giants. Duarte et al. (2013) found that Ro_ℓ controls reversal behavior in anelastic dynamos, particularly in cases with no-slip boundaries, for which reversals first appear above a critical value of Ro_ℓ.

7. Discussion

Limits on the generality of our results stem from the restricted class of dynamos we have considered. Our study uses thermochemical dynamos with relatively large magnetic Prandtl and Ekman numbers and the geometry of Earth's present-day core. We do not consider, for example, the effects of inner core heterogeneity or outer core layering, among other possible complications. In addition, the distinction between reversals and polarity excursions is based on subjective criteria (Kutzner and Christensen, 2004). Furthermore, our results do not imply that Ro_ℓ is the only similarity parameter for reversals, or even the best one. Reversal behavior might be systematized in terms of other factors such as zonal flows, polar wander (Biggin et al., 2012), the relative thicknesses of viscous and thermal boundary layers (King et al., 2009), or other dimensionless parameters, such as a modified Rayleigh number (Driscoll and Olson, 2009a). In addition, it was argued that inertia, which plays an important role in reversing dynamo models, is less important in Earth's core because scales smaller than the Rhines length scale do not affect the dynamo process (Sreenivasan and Jones, 2006).

In particular, one complication that has not been addressed in this study is the impact of the magnetic condition on the inner boundary. Lhuillier et al. (2013) argued that inner core conductivity may play an important role in determining the dynamo regime. They found that reversals in dynamo models with a conducting inner core are much less systematic and more frequent than in dynamo models with an insulating inner core. In contrast, other studies found that inner core conductivity has no apparent impact on reversal frequency (Wicht, 2002; Wicht, 2005), while still others find it tends to stabilize the dipole (Dharmaraj and Stanley, 2012). These apparently conflicting results indicate that the effect of inner core conductivity is highly parameter-dependent, and may not be systematic from one dynamo model to another.

Nevertheless, within the class of dynamos we examine, our results demonstrate that Ro_ℓ scales reversal frequency. In addition, we can point to evidence that our results have qualitative applicability beyond the parameter regime we have tested here. Table 1 includes statistics from two smaller Ekman number thermochemical dynamos ($E = 3 \times 10^{-4}$, cases U4) with uniform boundary conditions that were run for 400 and $278\tau_d$, respectively, from a study by Olson et al. (2012). The longer running, lower Rayleigh number case with $Ro_\ell \simeq 0.035$ did not reverse, whereas the higher Rayleigh number case with $Ro_\ell \simeq 0.075$ reversed five times. These results are qualitatively consistent with our higher Ekman number thermochemical dynamos, although there are too few dynamo cases with too few reversals at this lower Ekman number to determine if they obey the same reversal scaling relationships we have derived.

For heterogeneous CMB heat flux, reversal scaling is complicated by spatial heterogeneity of the convection. For example, if $Ro_\ell < Ro_{\ell crit}$ in one part of the outer core and $Ro_\ell > Ro_{\ell crit}$ in another, reversals might be initiated in these latter regions, even if the globally averaged Ro_ℓ is subcritical. We have argued that, for some patterns of heterogeneous CMB heat flux, it is appropriate to correct the local Rossby number using the maximum CMB heat flux, thereby accounting for the smallest eddy sizes and highest velocities. Using the heterogeneity-corrected local Rossby number Ro'_ℓ defined in (19), we show that the reversal frequencies in our tomographic dynamos conform to those from our uniform dynamos.

Compatibility between the underlying convection and the pattern of CMB heat flux is another complicating factor, particularly in cases with zonal boundary heterogeneity. We argue that close to the onset of convection, geographic control dominates and equatorial cooling tends to increase reversal frequency via low-latitude flux concentration, whereas far from onset, inertial control dominates and reversal frequency depends on the compatibility between the convection and the boundary heterogeneity. This offers a possible explanation for the phenomenon of polarity stabilization reported in previous studies with zonal CMB heterogeneity (Glatzmaier et al., 1999; Kutzner and Christensen, 2004). Amit et al. (2010) proposed several end-member scenarios for reversals that include these effects, one involving dipole rotation with little or no decrease in dipole magnitude, in which the axial dipole energy is transferred to the equatorial dipole, and a second involving dipole collapse, in which either the dipole energy cascades to smaller scales (Amit and Olson, 2010; Huguet and Amit, 2012) or the entire field decays to a minimum. Elements of both scenarios have been identified in reversing dynamos, in particular, equatorial dipole maximum for the dipole rotation scenario and dipole intensity minimum for the dipole collapse scenario (e.g. Olson et al., 2009). The present study suggests that dipole rotation is characteristic of reversals with geographic control, whereas dipole collapse is characteristic of reversals with inertial control.

Acknowledgments

This research was supported by Frontiers in Earth System Dynamics grant EAR-1135382 from the National Science Foundation. We are grateful to Alex Fournier and Binod Sreenivasan for their constructive reviews. We thank Gaël Choblet for insightful discussions.

References

Amit, H., Christensen, U., Langlais, B., 2011. The influence of degree-1 mantle heterogeneity on the past dynamo of Mars. Phys. Earth Planet. Inter. 189, 63–79.
Amit, H., Leonhardt, R., Wicht, J., 2010. Polarity reversals from paleomagnetic observations and numerical dynamo simulations. Space Sci. Rev. 155, 293–335.
Amit, H., Olson, P., 2006. Time-average and time-dependent parts of core flow. Phys. Earth Planet. Inter. 155, 120–139.
Amit, H., Olson, P., 2010. A dynamo cascade interpretation of the geomagnetic dipole decrease. Geophys. J. Int. 181, 1411–1427.
Aubert, J., 2005. Steady zonal flows in spherical shell fluid dynamos. J. Fluid Mech. 542, 53–67.
Aubert, J., Labrosse, S., Poitou, C., 2009. Modelling the paleo-evolution of the geodynamo. Geophys. J. Int. 179, 1414–1428.
Berhanu, M., Monchaux, R., Fauve, S., Mordant, N., Petrelis, F., Chiffaudel, A., Daviaud, F., Dubrulle, B., Marie, L., Ravelet, F., Bourgoin, M., Odier, P., Pinton, J.F., Volk, R., 2007. Magnetic eld reversals in an experimental turbulent dynamo. Europhys. Lett. 77. http://dx.doi.org/10.1209/0295-5075/77/59001.
Biggin, A.J., Steinberger, B., Aubert, J., Suttie, N., Holme, R., Torsvik, T.H., van der Meer, D.G., van Hinsbergen, D.J.J., 2012. Possible links between long-term geomagnetic variations and whole-mantle convection processes. Nature Geosci. 5, 526–533.
Braginsky, S.I., Roberts, P.H., 1995. Equations governing convection in Earth's core and the geodynamo. Geophys. Astrophys. Fluid Dyn. 79, 1–97.
Cande, S., Kent, D., 1995. Revised calibration of the geomagnetic polarity timescale for the late Cretaceous and Cenozoic. J. Geophys. Res. (Solid Earth) 100 (4), 6093–6095.
Christensen, U., Aubert, J., 2006. Scaling properties of convection-driven dynamos in rotating spherical shells and application to planetary magnetic fields. Geophys. J. Int. 166, 97–114.
Christensen, U., Aubert, J., Hulot, G., 2010. Conditions for Earth-like geodynamo models. Earth Planet. Sci. Lett. 296, 487–496.
Christensen, U., Olson, P., Glatzmaier, G., 1998. A dynamo model interpretation of geomagnetic field structures. Geophys. Res. Lett. 25, 1565–1568.
Christensen, U., Wicht, J., 2007. Numerical dynamo simulations. In: Olson, P. (Ed.), Treatise on Geophysics, vol. 8. Elsevier Science.
Davidson, P.A., 2001. An Introduction to Magnetohydrodynamics. Cambridge University Press, Cambridge, UK.
Dharmaraj, G., Stanley, S., 2012. Effect of inner core conductivity on planetary dynamo models. Phys. Earth Planet. Inter. 212–213, 1–9.
Dietrich, W., Wicht, J., 2013. A hemispherical dynamo model: Implications for the Martian crustal magnetization. Phys. Earth Planet. Inter. 217, 10–21.
Driscoll, P.E., Olson, P.L., 2009a. Effects of buoyancy and rotation on the polarity reversal frequency of gravitationally-driven numerical dynamos. Geophys. J. Int. 178, 1337–1350.
Driscoll, P.E., Olson, P.L., 2009b. Polarity reversals in geodynamo models with core evolution. Earth Planet. Sci. Lett. 282 (1–4), 24–33.
Driscoll, P.E., Olson, P.L., 2011. Superchron cycles driven by variable core heat flow. Geophys. Res. Lett. 38 (9), L09304.
Elsasser, W.M., 1956. Hydromagnetic dynamo theory. Rev. Mod. Phys. 28, 135–163.
Finlay, C.C., Amit, H., 2011. On flow magnitude and field-flow alignment at Earth's core surface. Geophys. J. Int. 186, 175–192.
Gastine, T., Duarte, L., Wicht, J., 2012. Dipolar versus multipolar dynamos: the influence of the background density stratification. Astronom. Astrophys. 546, A19.
Duarte, L.D., Gastine, T., Wicht, J., 2013. Anelastic dynamo models with variable electrical conductivity: An application to gas giants. Phys. Earth Planet. Inter. 222, 22–34.
Gissinger, C., Dormy, D., Fauve, S., 2010. Morphology of field reversals in turbulent dynamos. Europhys. Lett. 90, 49001.
Glatzmaier, G., Coe, R., Hongre, L., Roberts, P., 1999. The role of the earth's mantle in controlling the frequency of geomagnetic reversals. Nature 401, 885–890.
Glatzmaier, G.A., Roberts, P.H., 1997. Simulating the geodynamo. Contemp. Phys. 38, 269–288.
Gubbins, D., Davies, C.J., 2013. The stratified layer at the core–mantle boundary caused by barodiffusion of oxygen, sulphur and silicon. Phys. Earth Planet. Inter. 215, 21–28.
Heimpel, M.H., Evans, M.E., 2013. Testing the geomagnetic dipole and reversing dynamo models over Earth's cooling history. Phys. Earth Planet. Inter. 224, 124–131.
Helffrich, G., Kaneshima, S., 2010. Outer-core compositional stratification from observed core wave speed profiles. Nature 468, 807–810.
Holme, R., 2007. Large-scale flow in the core. In: Olson, P. (Ed.), Treatise on Geophysics, vol. 8. Elsevier Science.
Hori, K., Wicht, J., Christensen, U.R., 2010. The effect of thermal boundary conditions on dynamos driven by internal heating. Phys. Earth Planet. Inter. 182, 85–97. http://dx.doi.org/10.1016/j.pepi.2010.06.011.
Huguet, L., Amit, H., 2012. Magnetic energy transfer at the top of the Earth's core. Geophys. J. Int. 190, 856–870.
Jonkers, A., 2003. Long-range dependence in the Cenozoic reversal record. Phys. Earth Planet. Inter. 135, 253–266.
King, E.M., Stellmach, S., Noir, J., Hansen, U., Aurnou, J.M., 2009. Boundary layer control of rotating convection systems. Nature 457, 301–304.
Kutzner, C., Christensen, U.R., 2000. Effects of driving mechanisms in geodynamo models. Geophys. Res. Lett. 27 (1). http://dx.doi.org/10.1029/1999GL010937.
Kutzner, C., Christensen, U.R., 2002. From stable dipolar towards reversing numerical dynamos. Phys. Earth Planet. Inter. 131, 29–45.
Kutzner, C., Christensen, U.R., 2004. Simulated geomagnetic reversals and preferred virtual geomagnetic pole paths. Geophys. J. Int. 157, 1105–1118.
Labrosse, S., 2003. Thermal and magnetic evolution of the earth's core. Phys. Earth Planet. Inter. 140, 127–143.
Landeau, M., Aubert, J., 2011. Equatorially antisymmetric convection inducing a hemispherical magnetic eld in rotating spheres and implications for the past martian dynamo. Phys. Earth Planet. Inter. 185, 61–73.
Layer, P.W., Kroner, A., McWilliams., M., 1996. An Archean geomagnetic reversal in the Kaap Valley pluton South Africa. Science 273, 943–946.
Lhuillier, F., Hulot, G., Gallet, Y., 2013. Statistical properties of reversals and chrons in numerical dynamos and implications for the geodynamo. Phys. Earth Planet. Inter. 220, 19–36.
Merrill, R.T., McElhinny, M.W., McFadden, P.L., 1998. The Magnetic Field of the Earth: Paleomagnetism, the Core, and the Deep Mantle. Academic Press, San Diego, California, USA.
Moffatt, H.K., 1978. Magnetic Field Generation in Electrically Conducting Fluids. Cambridge University Press, Cambridge, U.K.
Nimmo, F., 2007. Energetics of the core. In: Olson, P. (Ed.), Treatise on Geophysics, vol. 8. Elsevier Science.
Olson, P., Christensen, U., 2002. The time averaged magnetic field in numerical dynamos with nonuniform boundary heat flow. Geophys. J. Int. 151, 809–823.

Olson, P., Christensen, U., 2006. Dipole moment scaling for convection-driven planetary dynamos. Earth Planet. Sci. Lett. 250, 561–571.
Olson, P., Christensen, U., Driscoll, P., 2012. From superchrons to secular variation: A broadband dynamo frequency spectrum for the geomagnetic dipole. Earth Planet. Sci. Lett. 319–320, 75–82.
Olson, P., Christensen, U.R., Glatzmaier, G.A., 1999. Numerical modeling of the geodynamo: Mechanisms of field generation and equilibration. J. Geophys. Res. 104, 10383–110404.
Olson, P., Deguen, R., Hinnov, L.A., Zhong, S., 2013. Controls on geomagnetic reversals and core evolution by mantle convection in the Phanerozoic. Phys. Earth Planet. Inter. 214, 87–103.
Olson, P., Driscoll, P., Amit, H., 2009. Dipole collapse and reversal precursors in a numerical dynamo. Phys. Earth Planet. Inter. 173, 121–140.
Olson, P.L., Coe, R.S., Driscoll, P.E., Glatzmaier, G.A., Roberts, P.H., 2010. Geodynamo reversal frequency and heterogeneous core–mantle boundary heat flow. Phys. Earth Planet. Inter. 180, 66–79.
Pavlov, V., Gallet, Y., 2010. Variations in geomagnetic reversal frequency during the Earth's middle age. Geochem. Geophys. Geosyst. 11 (1).
Pétrélis, F., Besse, J., Valet, J.P., 2011. Plate tectonics may control geomagnetic reversal frequency. Geophys. Res. Lett. 38, L19303.
Pétrélis, F., Fauve, S., Dormy, E., Valet, J.P., 2009. Simple mechanism for reversals of Earth's magnetic field. Phys. Rev. Lett. 102, 144503.
Pozzo, M., Davies, C., Gubbins, D., Alfè, D., 2012. Thermal and electrical conductivity of iron at Earth's core conditions. Nature 485, 355–358.
Roberts, P.H., 2007. Theory of the geodynamo. In: Olson, P. (Ed.), Treatise on Geophysics, vol. 8. Elsevier Science.
Ryan, D.A., Sarson, G.R., 2007. Are geomagnetic field reversals controlled by turbulence within the Earth's core? Geophys. Res. Lett. 34, L02307. http://dx.doi.org/10.1029/2006GL028291.
Sreenivasan, B., Jones, C.A., 2006. The role of inertia in the evolution of spherical dynamos. Geophys. J. Int. 164, 467–476.
Stanley, S., Elkins-Tanton, L., Zuber, M.T., Parmentier, E.M., 2008. Mars' paleomagnetic field as the result of a single-hemisphere dynamo. Science 321, 1822–1825.
Strik, G., Blake, T.S., Zegers, T.E., White, S.H., Langereis, C.G., 2003. Palaeomagnetism of flood basalts in the Pilbara Craton, Western Australia: Late Archaean continental drift and the oldest known reversal of the geomagnetic field. J. Geophys. Res. 108 (B12), 2551.
Valet, J.P., Meynadier, L., Guyodo, Y., 2005. Geomagnetic dipole strength and reversal rate over the past two million years. Nature 435, 802–805.
Wicht, J., 2002. Inner-core conductivity in numerical dynamo simulations. Phys. Earth Planet. Inter. 132, 281–302.
Wicht, J., 2005. Palaeomagnetic interpretation of dynamo simulations. Geophys. J. Int. 162, 371–380.
Wicht, J., Stellmach, S., Harder, H., 2009. Numerical models of the geodynamo: From fundamental Cartesian models to 3D simulations of field reversals. In: Glassmeier, H., Soffel, H., Negendank, J. (Eds.), Geomagnetic Field Variations - Space-time structure, processes, and effects on system Earth. Springer, Berlin.
Wilks, D.S., 2006. Statistical methods in the atmospheric sciences. Academic Press, US.
Zhang, N., Zhong, S., 2011. Heat fluxes at the Earth's surface and core–mantle boundary since Pangea formation and their implications for the geomagnetic superchrons. Earth Planet. Sci. Lett. 306, 205–2016.
Ziegler, L.B., Constable, C.G., Johnson, C.L., Tauxe, L., 2011. PADM2M: a penalized maximum likelihood model of the 02 Ma palaeomagnetic axial dipole moment. Geophys. J. Int. 184 (3), 1069–1089.